Title

Binary Rare-Earth Silicate Glasses Near Deep Eutectic: The Case for Sc_2O_3—SiO_2 System

Journal

Journal of the American Ceramic Society, 109(5)

ISSN

0002-7820

Authors

Everson, Bryce

Chuang, Shih-Yi

Hung, Ivan

et al.

Publication Date

2026-05-01

DOI

10.1111/jace.70869

Peer reviewed

Journal of the American Ceramic Society

RESEARCH ARTICLE

Binary Rare-Earth Silicate Glasses Near Deep Eutectic: The Case for Sc_2O_3–SiO_2 System

Bryce Everson[1] | Shih-Yi Chuang[1] | Ivan Hung[2] | Zhehong Gan[2] | Scott J. McCormack[1] | Sabyasachi Sen[1]

[1]Deparment of Materials Science and Engineering, University of California at Davis, Davis, California, USA | [2]National High Magnetic Field Laboratory, Tallahassee, Florida, USA

Correspondence: Sabyasachi Sen (sbsen@ucdavis.edu)

Received: 3 March 2026 | **Revised:** 25 April 2026 | **Accepted:** 12 May 2026

ABSTRACT

Homogeneous glass formation in binary rare-earth silicate systems has thus far been precluded due to the presence of extensive liquid–liquid immiscibility and a strong tendency of these liquids toward crystallization. In this study, we demonstrate homogeneous glass formation in the Sc_2O_3–SiO_2 binary system within a narrow compositional window (37–39 mol% Sc_2O_3) near a deep eutectic between the compounds $Sc_2Si_2O_7$ and Sc_2SiO_5, using containerless laser melting under aerodynamic levitation. The atomic structure of these unusual glasses is investigated using multinuclear (^{29}Si, ^{45}Sc, ^{17}O) solid-state nuclear magnetic resonance (NMR) and Raman spectroscopy. The spectroscopic results, when taken together, provide a comprehensive picture of the structure of these glasses characterized by pyrosilicate $[Si_2O_7]^{6-}$ anionic units interconnected by Sc cations in ScO_6 coordination polyhedra, via Si–O–Sc linkages. A significant fraction (~6%) of the oxygen atoms in the structure is present as free oxide (FO) ions in Sc–O–Sc linkages, providing connectivity between the ScO_6 polyhedra. The formation of the FO species via oxygen disproportionation reaction is promoted by the uniquely high field strength of the Sc^{3+} ions, and the resulting structural frustration is hypothesized to suppress crystallization of the stable pyrosilicate phase in these liquids, enabling glass formation in an otherwise non-glass-forming binary system. These findings highlight the critical role of rare-earth cation field strength in controlling oxygen speciation, structure, and glass-forming ability in this binary silicate system.

1 | Introduction

Rare-earth (RE = lanthanides, Y and Sc) ions constitute an important class of additive that have been used either as dopants or as major components in oxide network glasses for imparting relatively unique physical properties that are relevant to technological applications ranging from photonics to encapsulation of radioactive waste. Specifically, the incorporation of RE ions results in significant enhancement in optical (refractive index, tunable colors/luminescence, lasing), thermal (high glass transition temperature T_g and low thermal expansion coefficient), chemical (corrosion resistance), and mechanical (high microhardness) properties [1–10]. A number of these properties show systematic and monotonic change with the mass and the field strength of the RE cations [3], where the latter is a function of the charge Z and the radius r of the cation and is given by Z/r^2. In comparison with the typical network-modifier cations such as the alkalis and most of the alkaline earths (excluding Mg^{2+} in fourfold coordination), the RE cations with $Z = 3$ are characterized by significantly higher field strength (HFS) with the smallest RE Sc^{3+} having the highest field strength. HFS cations are also known to promote disproportionation of Si Q^n species in the glass structure driving Reaction (2) $Q^n \rightarrow Q^{n-1} + Q^{n+1}$, where n denotes the number of bridging oxygen (BO) atoms on an SiO_4 tetrahedron [11]. Moreover, these cations also promote the formation of fivefold and sixfold coordinated Al species in aluminosilicate glasses [12]. Such behavior of HFS cations stems from their strong affinity for bonding to negatively charged

oxygen atoms in the structure that is, of course, maximized in the case of network formers such Si^{4+} or P^{5+}, characterized by some of the highest field strengths.

Finally, besides *Q*-species disproportionation, the HFS cations are also expected to favor the oxygen disproportionation reaction: 2NBO → free oxide (FO) + BO, where NBO denotes a non-BO atom that is linked to one network-forming cation and several network-modifier cations, whereas FO corresponds to the FO ion, that is, an oxygen that is not linked to any network-forming cation in the structure [13]. These speciation equilibria strongly influence the structure of the glass-forming liquid, thermodynamics, and properties such as viscosity and fragility. In highly modified systems, FO becomes unavoidable once the oxygen-to-network-former atomic ratio exceeds the value *N* required to satisfy the formation of isolated cation-oxygen polyhedra (e.g., $N > 3$ for BO_3 triangles or $N > 4$ SiO_4 tetrahedra, in borates and silicates, respectively), although small amounts of FO may appear even slightly below these thresholds due to entropic stabilization [13]. Direct observation of FO formation has indeed been made only in highly modified RE-borate and Pb-silicate glasses as well as in Ca–Mg silicate glasses near the orthosilicate composition using ^{17}O nuclear magnetic resonance (NMR) spectroscopy [13–15]. Moreover, small amount of FO formation in RE-aluminosilicate glasses has been claimed to be necessary to explain certain non-monotonic variations in physical properties and would be consistent with the molecular dynamics simulation results, although no direct spectroscopic observation of such oxygen species has been reported in the literature [3].

Oxygen speciation in highly modified oxide glasses remains a poorly explored area because of synthesis challenges. Recent containerless processing has enabled glass formation in RE-borate systems with exceptionally high modifier contents, providing an opportunity to directly probe oxygen and boron speciation [8–10, 13]. However, to the best of our knowledge, no glass formation has been reported in simple binary RE-silicate (RE_2O_3–SiO_2) systems to date. These binary systems are characterized by a large immiscibility dome that spans the region between 100 mol% SiO_2 and ~70 to 80 mol% SiO_2, rendering homogeneous glass formation practically impossible [16–19]. The adverse effect of this immiscibility is well known in the RE doping of silica glass for applications in fiber amplifier technology for all-optical telecommunications networks. Doping at the level of even a few hundred to a few thousand parts per million of RE-oxide into silica results in clustering of rare-earth ions and consequent fluorescence quenching, which is severely detrimental to the optical amplification efficiency [20, 21].

Further lowering of SiO_2 content to below 80 mol% results in the appearance of two eutectics in the RE_2O_3–SiO_2 phase diagram that are located near ~70 and ~40 mol% SiO_2 [16–19]. The former composition close to the stoichiometry of $RE_2Si_2O_7$ corresponds to the lowest melting point in the system. In the present study, we have explored glass formation in the Sc_2O_3–SiO_2 binary system using containerless processing by laser melting under aerodynamic levitation, thus minimizing the possibility of heterogeneous nucleation-induced crystallization of the melt on cooling. We report the formation of optically homogeneous glasses in this system in a rather narrow composition range between ~37 and 39 mol% Sc_2O_3, close to, but not coincident

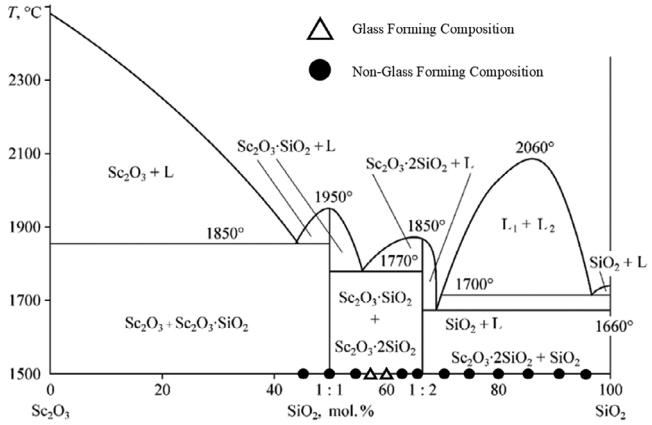

FIGURE 1 | Sc_2O_3–SiO_2 binary phase diagram [19] annotated with glass-forming ability of the investigated compositions. Filled circles indicate nominal, that is, batched compositions that undergo partial to complete crystallization upon quenching, whereas open triangles correspond to those that form homogeneous glass. Note that analyzed compositions of these homogeneous glasses show loss of ~3 mol% Sc_2O_3 during melting.

with, one of the deep eutectics in the phase diagram near the composition with ~43 mol% Sc_2O_3, located between the compounds Sc_2SiO_5 and $Sc_2Si_2O_7$, the latter of which is incidentally also found in nature as the mineral thortveitite. We present the results of a comprehensive structural study of these glasses using multinuclear (^{29}Si, ^{45}Sc, and ^{17}O) NMR spectroscopy and explore the unique structural role of the highest field strength RE cation Sc^{3+} in the glass structure.

2 | Experimental Details

2.1 | Glass Synthesis

$(Sc_2O_3)_x(SiO_2)_{1-x}$ glass beads within the compositional window $0.05 \leq x \leq 0.55$ were fabricated in 5 mol% increments to determine the glass-forming region in the Sc_2O_3–SiO_2 binary system. Stoichiometric amounts of the constituent oxides (99.99% Sc_2O_3, MSE Supplies and 99.998% SiO_2, Thermo Scientific) were thoroughly mixed and ground in a mortar and pestle to produce homogeneous powder batches. Each batch was loaded into a copper hearth containing spherical wells and melted using a 400 W CO_2 laser (10.6 μm; Synrad PSi401SB; Mukilteo, WA) forming spherical crystalline beads approximately 2 mm in diameter. Following laser consolidation, the spheres were levitated in an oxygen atmosphere, laser heated to ~2100°C, allowed to equilibrate, and subsequently quenched by powering off the laser.

The crystallinity of the resulting beads was assessed with powder x-ray diffraction to identify the glass-forming region of the binary system. From these experiments, nominally batched compositions with $x = 0.40$–0.42 were able to form glass, as illustrated in Figure 1. The final compositions of the glass beads after laser processing were determined using x-ray fluorescence (XRF) spectroscopy (Rigaku Supermini200). Elemental analysis revealed that the true glass-forming region corresponds to $0.37 \leq x \leq 0.39$, which is located close to the stoichiometry of $Sc_2Si_2O_7$ ($x = 0.33$) and to the location of the deep eutectic between this composition

and Sc_2SiO_5 in the phase diagram near $x \sim 0.43$ (Figure 1). The atomic structure and thermophysical properties of two glasses with $x = 0.37$ and 0.39 are investigated in this study, and these two compositions are denoted as Sc-37 and Sc-39, respectively, in the subsequent discussion.

After establishing the glass-forming region, an Sc-37 glass sample enriched in ^{17}O isotope was synthesized for ^{17}O NMR spectroscopic measurements. This glass was synthesized using the standard Sc_2O_3 powder and a 1:1 by weight mixture of natural-abundance SiO_2 and that isotopically enriched with ^{17}O. The isotopically enriched SiO_2 was prepared by hydrolyzing $SiCl_4$ with 60% enriched $H_2{}^{17}O$ following standard procedure reported in previous studies in the literature [22].

2.2 | Physical Properties

The glass transition and crystallization behavior of the Sc-37 and Sc-39 glasses were probed using a differential scanning calorimeter (NETZSCH STA 449F5). For each composition, one or two glass spheres (10–15 mg) were placed in an alumina crucible. The samples were heated at 10 K/min under a nitrogen atmosphere, and data were collected during this upscan. Although both Sc-37 and Sc-39 glasses showed a relatively sharp crystallization exotherm centered at 986°C, no clear endothermic signal corresponding to glass transition was observed. This apparent absence of a clear glass transition is not unusual for glasses whose parent melts are highly fragile and unstable against crystallization on supercooling; the orthosilicate Mg_2SiO_4 glass with its notoriously poor glass-forming ability is a case in point [23]. Such glasses typically undergo rapid nucleation and crystallization as the glass transition temperature T_g is reached on heating, and the relaxation time of the resulting supercooled liquid drastically decreases rendering the constituent atoms highly mobile at the experimental timescale. In these cases, T_g is often approximated to be the same as the temperature of the onset of crystallization [23]. In fact, a closer inspection of the DSC scans of the Sc-silicate glasses in Figure 2 indeed appears to show the hint of an onset of the glass transition endotherm near 950°C. The density of these glasses was measured using He-gas displacement pycnometry and was found to be 3.371 ± 0.004 and 3.420 ± 0.002 g/cm^3, respectively, for Sc-37 and Sc-39 glasses. The corresponding molar volumes calculated using an oxide basis are ~26.37 and ~26.44 cm^3, respectively. The density and molar volume values are comparable to those reported for Sc-aluminosilicate glasses by Pahari et al. in a previous study. It may be noted here for comparison that crystalline $Sc_2Si_2O_7$ with 33.33% Sc_2O_3 has a density of 3.374 g/cm^3.

2.3 | NMR Spectroscopy

The ^{29}Si and ^{45}Sc magic-angle-spinning (MAS) NMR experiments were carried out using a Bruker Avance spectrometer equipped with a 11.7-T wide-bore magnet operating at the ^{29}Si (^{45}Sc) Larmor frequency of 99.3 (121.5) MHz The ^{29}Si (^{45}Sc) MAS NMR spectra were acquired using a Bruker 4 mm (2.5 mm) MAS probe. The as-made spherical glass beads were crushed and taken into ZrO_2 rotors and spun at 12 kHz (32 kHz) for collection of ^{29}Si (^{45}Sc) NMR data. For ^{29}Si MAS NMR, approximately 2000 free induction

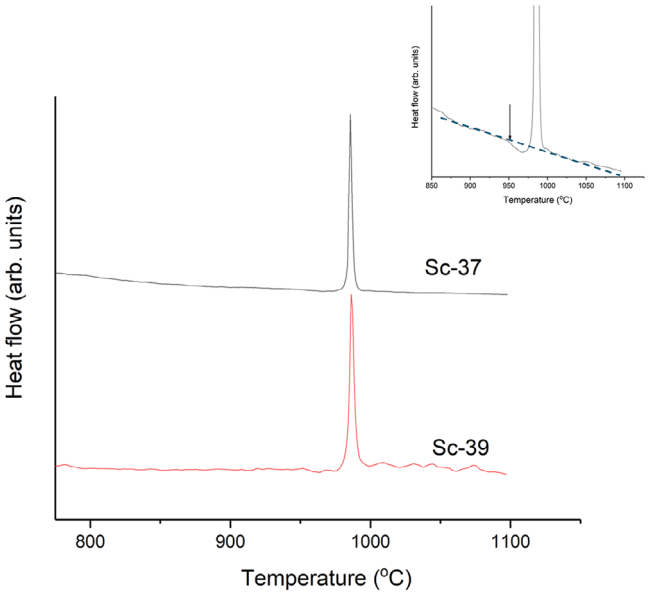

FIGURE 2 | DSC scans of Sc-37 (top) and Sc-39 (bottom) glasses. Sharp peak at 986°C corresponds to crystallization exotherm. Inset shows expanded view of top scan with an approximate baseline marked by the dashed line and a vertical arrow marking possible onset near 950°C of an endotherm corresponding to glass transition (see text for details).

decays (FIDs) were collected using a 60° pulse (1.7 μs) and 60 s recycle delay, averaged, and Fourier-transformed to obtain each spectrum. All ^{29}Si spectra were externally referenced to tetramethylsilane. The ^{45}Sc MAS NMR spectrum was collected using a solids 30° pulse (0.07 μs) and 0.2 s recycle delay. A total of 8600 FIDs were averaged and Fourier-transformed to obtain the spectrum. The ^{45}Sc NMR spectra were externally referenced to crystalline $LiScO_2$ (^{45}Sc chemical shift = 148 ppm [24]).

The ^{17}O MAS and triple-quantum (3Q) MAS NMR spectra, and ^{45}Sc QMATPASS/QCPMG NMR spectrum of the isotopically enriched Sc-37 glass were collected at the National High Magnetic Field Laboratory (NHMFL, Tallahassee, Florida) using a Bruker Avance NEO console operating at a magnetic field $B_0 = 20$ T (i.e., Larmor frequencies of 115.3 and 206.6 MHz for ^{17}O and ^{45}Sc) and a Low-E 3.2 mm HX MAS probe designed and constructed at the NHMFL. The glass sample was crushed and packed into a 3.2 mm ZrO_2 rotor and spun at 16 kHz. The ^{17}O MAS spectrum was acquired with a central-transition selective 30° flip-angle pulse of 1 μs at an rf field amplitude of 27.8 kHz, a 1 s recycle delay, and 8192 averaged transients. In addition, a WURST (Wideband-Uniform Rate-Smooth Truncation) pulse with 288 kHz offset and 15.4 kHz rf field was applied to the satellite transitions for enhancement of the central transition polarization [25, 26]. A shifted-echo SPAM MQMAS pulse sequence was used to acquire the 2D ^{17}O 3QMAS spectrum [27, 28]. Pulses of 3 and 1 μs were used for excitation and conversion of 3Q coherence with an rf amplitude of ~110 kHz, and selective $\pi/2$ and π pulses of 5 and 10 μs with rf field of 16.7 kHz. The indirect spectral window was rotor-synchronized by incrementing the t_1 delay by the rotor period, 62.5 μs. The 2D experiment employed a 2 s recycle delay, 1440 averaged transients per t_1 increment, 20 t_1 complex points acquired in the indirect dimension, and a total experiment time of 16 h.

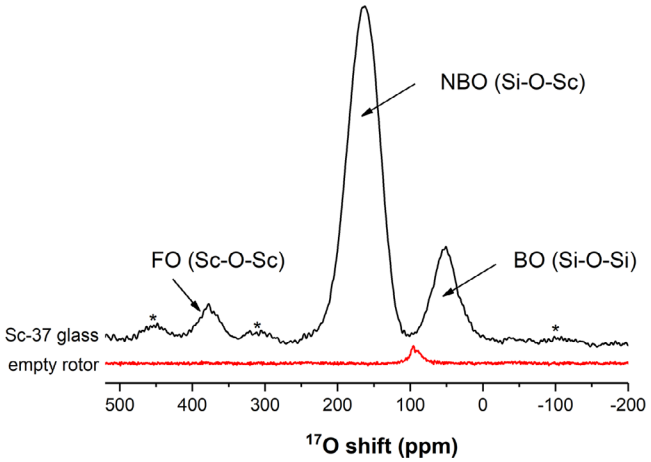

FIGURE 3 | ^{17}O MAS NMR spectrum of Sc-37 glass (top, black line) and of empty rotor background (bottom, red line) collected at 20.0 T. Structural assignments of constituent resonances to different oxygen sites in the glass spectrum are denoted with arrows. Asterisks denote spinning sidebands.

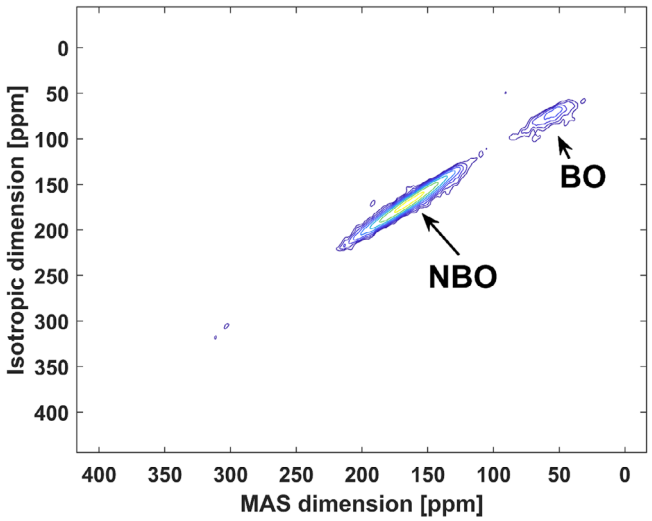

FIGURE 4 | ^{17}O 3QMAS NMR spectrum of Sc-37 glass collected at 20.0 T. NBO and BO resonances are denoted with arrows, whereas FO resonance was too weak to be observed.

The ^{45}Sc "infinite MAS" NMR spectrum was obtained using the method previously outlined by sum projection of a sheared 2D MAT/CPMG spectrum [25] but using the nine π-pulse [29], instead of the five π-pulse MAT pulse sequence. Acquisition of the 2D ^{45}Sc QMAT/QCPMG spectrum consisted of 16 hypercomplex t_1 increments, each with 100 transients, 0.2 s recycle delay, and a total experimental time of ~12 min. A total of 65 CPMG echoes were co-added for S/N improvement before the processing of 2D spectrum. The ^{17}O and ^{45}Sc spectra were externally referenced by recording the ^{17}O signal of natural abundance H_2O, setting it to 2.8 ppm with respect to the D_2O ^{17}O frequency at 0 ppm, and then using the appropriate frequency ratio reported in the IUPAC recommendations [30].

2.4 | Raman Spectroscopy

The Raman spectra of both glasses were collected in backscattered geometry using a Renishaw 1000 Raman microscope spectrometer equipped with a diode laser (Spectron Development Laboratories: SDL-8530) operating at a wavelength of 785 nm. The laser power was set to allow 10% transmission through the sample. The backscattered light was detected using a charge-coupled device cooled at 200 K.

3 | Results and Discussion

The ^{17}O central transition MAS NMR spectrum of the Sc-37 glass consists of three well-resolved resonances of approximately Gaussian shape centered at ~56, 164.5, and 375 ppm (Figure 3). The resonance at 56 ppm can be readily assigned to the Si–O–Si (i.e., BO) environment, whereas the strongest resonance at 164.5 ppm is consistent with the NBO environment in Si–O–Sc [31]. These two resonances are also apparent in the ^{17}O 3QMAS NMR spectrum (Figure 4). For a spin $I = 5/2$ nuclide such as ^{17}O, the δ_{iso} and the quadrupolar product $P_Q = C_Q\,(1+\eta^2/3)$ for the two resonances can be estimated from their isotropic peak position δ_{F_1} and their center of gravity $\delta_{F_2}^{CG}$ along the MAS dimension using the following relations [32]:

$$\delta_{iso} = \frac{17}{27}\,\delta_{F_1} + \frac{10}{27}\delta_{F_2}^{CG} \quad (1)$$

$$P_Q = \left[\left(\delta_{F_1} - \delta_{F_2}^{CG}\right)^{1/2}\right]\left(\frac{\nu_0}{1000}\right)\sqrt{\frac{680[2I\,(2I-1)]^2}{81\,[4I\,(I+1)-3]}} \quad (2)$$

where ν_0 is the resonance frequency (115.3 MHz), and $I = 5/2$ is the spin quantum number of the nuclide. Such calculations yield δ_{iso} and P_Q values of ~167.1 ppm and 2.6 MHz, respectively, for the NBO site and 65.7 ppm and 4.9 MHz, respectively, for the BO site. Finally, the ^{17}O chemical shift of 375 ppm for the downfield resonance is similar to that reported for Sc–O–Sc type FO environments in crystalline compounds Sc_2O_3 (340 ppm) and Sr_2ScGaO_5 (340–366 ppm) [33, 34]. It may be noted that the background from the empty rotor collected under identical conditions has only a weak ^{17}O NMR signal near ~90 ppm and thus has no significant contribution to the observed ^{17}O MAS NMR spectrum of the Sc-37 glass.

Integration of the peak areas for the NBO, BO, and FO resonances yields their relative fractions to be ~81%, 13%, and 6%, respectively. On the other hand, the chemical composition of the Sc36 glass indicates that if, on melting, all Sc–O–Sc type FO species in Sc_2O_3 react with the BO species (i.e., Si–O–Si) in SiO_2 and convert to NBO of the type Si–O–Sc via the reaction FO + BO → 2NBO then 93% of all oxygen atoms would have an NBO character, whereas the rest (7%) would be BO. Therefore, the experimentally observed oxygen speciation indicates that the high field strength of the Sc^{3+} ion favors the formation of FO environments, which can be expressed in the form of a conversion of 12% of the NBO into 6% BO and 6% FO following the reaction:

$$12\text{NBO} \rightarrow 6\text{FO} + 6\text{BO}$$

Moreover, the observation of 81% NBO in Sc-37 glass implies that out of 237 oxygen atoms in the formula unit $(Sc_2O_3)_{37}(SiO_2)_{63}$

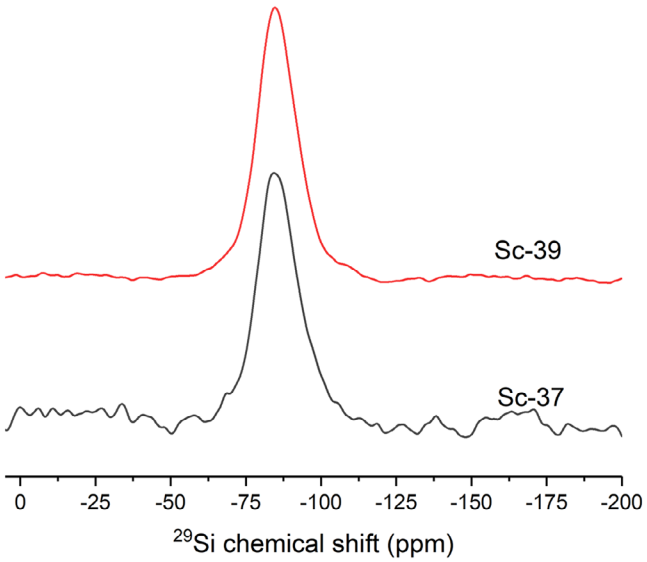

FIGURE 5 | ^{29}Si MAS NMR spectra of Sc-37 (bottom) and Sc-39 (top) glasses.

approximately 192 are NBO, and thus NBO/Si is ~3, which, in turn, suggests that the Si atoms should predominantly be present at Q^1 species, that is, as $[Si_2O_7]^{6-}$ dimers in the structure of this glass. This expectation can be verified against the ^{29}Si MAS spectra of the two glasses, which display a relatively symmetric and featureless resonance centered at approx. −85 ppm with a full width at half maximum of ~15 ppm (Figure 5). It may be noted here that typically the ^{29}Si isotropic chemical shift δ_{iso} ranges for the depolymerized Q^0, Q^1, and Q^2 species in various silicates can overlap significantly and depend, among other factors, on the type of the charge-balancing cations in the structure and on the Si–O–Si angle. For example, the ^{29}Si δ_{iso} for the Q^0 species in Mg_2SiO_4 is −61.9 ppm and in $ZrSiO_4$ is −81.6 ppm, whereas the ^{29}Si δ_{iso} for the Q^1 species in $Na_6Si_2O_7$ is −68.4 ppm and in $La_2Si_2O_7$ is −83.2 ppm, and for the Q^2 species the ^{29}Si δ_{iso} is −74.5 ppm for Li_2SiO_3 and −84.0 ppm for β-$Ca_3Si_3O_9$ [35].

It is intriguing to note here that the ^{29}Si δ_{iso} for the Q^1 species can span an even wider range in the case of $RE_2Si_2O_7$ compounds. The ^{29}Si δ_{iso} in these compounds with $[Si_2O_7]^{6-}$ anionic units becomes more negative with increasing ∠Si–O–Si angle between the two SiO_4 tetrahedra. For example, for $La_2Si_2O_7$ with ∠Si–O–Si = 133° the ^{29}Si δ_{iso} is −83.2 ppm, whereas it reaches a value of −95 ppm in the case of $Sc_2Si_2O_7$ and $Lu_2Si_2O_7$ with ∠Si–O–Si = 180° [36]. Therefore, the observed average ^{29}Si δ_{iso} of −85 ppm for these Sc-silicate glasses appears to be consistent with the structure consisting primarily of $[Si_2O_7]^{6-}$ anionic units with ∠Si–O–Si similar to that in $La_2Si_2O_7$.

The Sc–O coordination environment in these glasses can be probed with ^{45}Sc NMR spectroscopy [4, 36]. The ^{45}Sc MAS NMR spectra of the Sc-37 glass collected at two different magnetic fields of 11.7 and 20.0 T are presented in Figure 6A. The ^{45}Sc NMR line shape at low field does not change significantly between the Sc-37 and Sc-39 samples. The significant asymmetric broadening of the low-field ^{45}Sc MAS NMR spectral line shape with a low-frequency tail is typical of line shapes of quadrupolar nuclides in glasses and suggests that at this field the line shape is dominated by a distribution of the ^{45}Sc quadrupolar coupling constant C_Q. This type of NMR line shapes can be simulated well with a Czjzek distribution of disorder that results in a normal distribution of electric field gradient tensor elements at the site of the nucleus. Such a simulation (Figure 6A) yields a ^{45}Sc NMR δ_{iso} ~105 ppm and of C_Q ~ 21 MHz, both typical of Sc in sixfold coordination [24]. A similar coordination environment for Sc was also proposed to be present in the structure of Sc-aluminosilicate glasses by Eden and coworkers on the basis of ^{45}Sc NMR spectroscopy [4, 36].

The large C_Q of ^{45}Sc and additional isotropic shift distribution resulted in a rather broad center band, which made the applied MAS frequency of 16 kHz insufficient to get a clean ^{45}Sc NMR center band (free of overlap with spinning sidebands) spectral line shape at the higher field (Figure 6A). The QMAT experiment was thus used to help separate the MAS center band from the spinning sidebands, including those arising from the quadrupolar interaction. The quadrupolar line broadening in ppm scale is expected to decrease with increasing magnetic field B_0 as $(B_0)^{-2}$. However, the linewidth of the ^{45}Sc QMAT/QCPMG NMR spectrum obtained at 20.0 T only decreases by 25% compared to the width of the MAS spectrum obtained at 11.7 T (Figure 6B), which suggests that a significant part of the ^{45}Sc NMR linewidth at 20.0 T is associated with chemical shift distribution. This high-field line shape can also be simulated with a Czjzek distribution with similar parameters as those used for the simulation of the low-field line shape (δ_{iso} ~ 105 ppm and C_Q ~ 24.0 MHz); however, only with a chemical shift distribution that is twice as large for the former compared to that required for the latter.

It may be noted that a measure of the strength of an interatomic bond is its bond valence (BV), and the BV of an Sc–O bond for ^{VI}Sc in its typical octahedral (sixfold) coordination is ~0.50 to 0.60, which is similar to that of an Al–O bond for ^{V}Al in fivefold coordination (~0.55 to 0.60) [37–39]. These values can be compared to the BV of an Al–O bond for ^{IV}Al in tetrahedral coordination (~0.75 to 0.80) and ^{VI}Al in octahedral coordination (0.45 to 0.50) [38, 39]. A network-forming cation (e.g., Si, P) can be defined to be one so that only two such cations can bond to an oxygen atom equally or subequally to satisfy the BV sum requirement to be ~2.0 within 10%–20%. The BV sum for an ^{V}Al–O–Si or an ^{VI}Al–O–Si linkage (~1.5 to 1.6) is substantially lower than 2.0, and the oxygen atom will bond to a third ^{V}Al or ^{VI}Al ion. Therefore, ^{V}Al or ^{VI}Al behaves as a network modifier, similar to ^{VI}Sc in the Sc-silicate glasses. This scenario implies that all NBO in the structure will be bonded to 1 Si and 2 Sc atoms. Considering Si and Sc to be four- and six-coordinated and avoiding double counting, each NBO is linked to 1/4 Si and 2/6 Sc. Therefore, the 192 NBO in the formula unit $(Sc_2O_3)_{37}(SiO_2)_{63}$, as determined via ^{17}O NMR satisfies the bonding requirement for approximately 64 Sc atoms. The remaining 10 Sc atoms per formula unit then must form Sc–O–Sc linkages, and considering the BV of Sc–O bond to be ~0.55, each FO would need to be bonded to 4 Sc nearest neighbors in $O(Sc)_4$ configuration as observed in crystalline Sc_2O_3. Therefore, each FO will satisfy the bonding requirement of 4/6 Sc and thus would predict a total of 15 FO (6.3%) per formula unit. This prediction is then consistent with the ^{17}O NMR result, which indicates that ~6% of all oxygen atoms in the structure are present as FO.

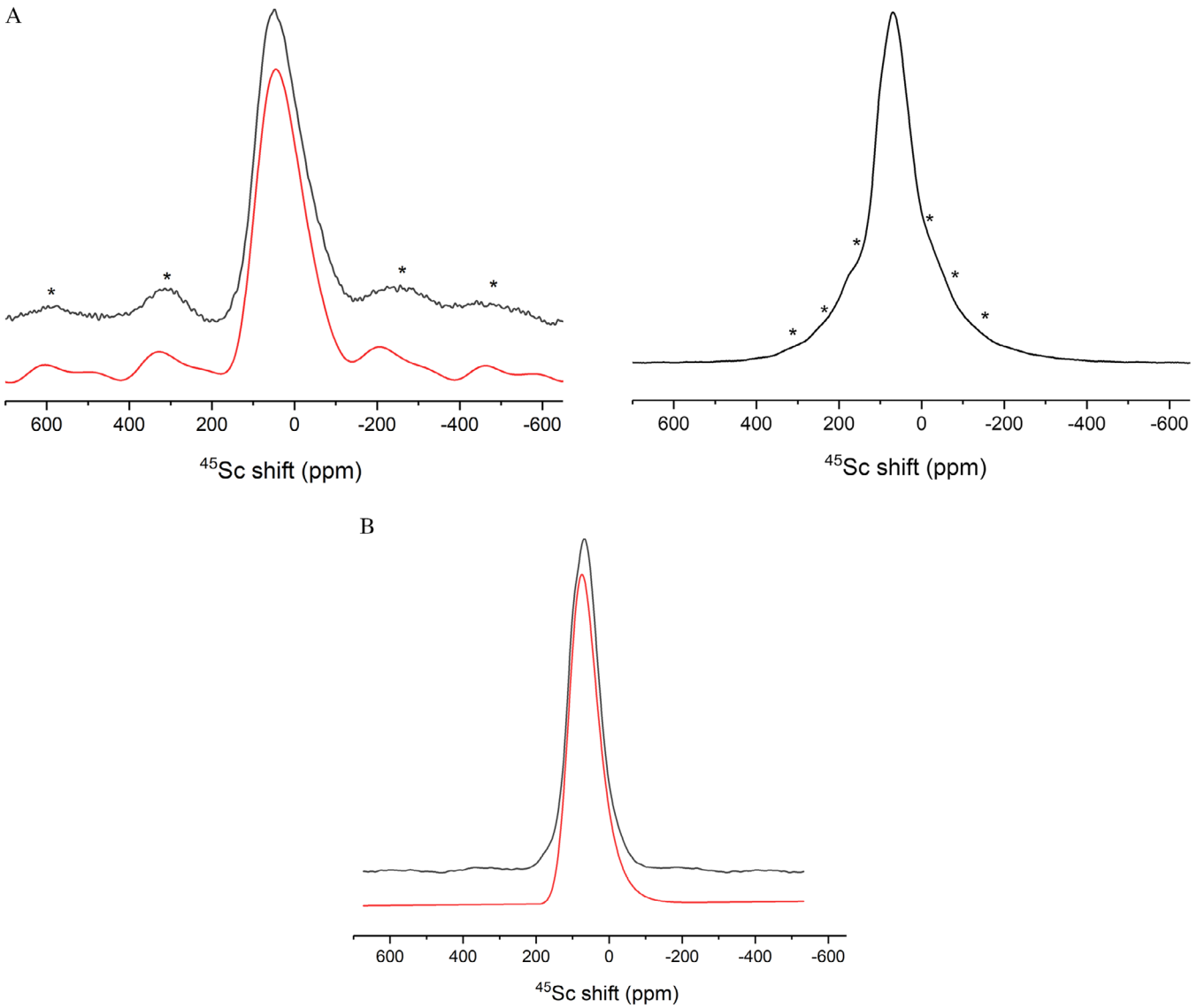

FIGURE 6 | (A) Top figure- Left: Experimental (top: black line) and simulated (bottom: red line) ^{45}Sc MAS NMR spectra of Sc-37 glass collected at 11.7 T at a spinning speed of 32 kHz. Right: Experimental ^{45}Sc MAS NMR spectra of Sc-37 glass collected at 20.0 T at a spinning speed of 16 kHz. Asterisks denote spinning sidebands. (B) Bottom figure- Experimental (top: black line) and simulated (bottom: red line) "infinite MAS" ^{45}Sc NMR spectrum of Sc-37 glass collected at 20.0 T obtained from sum-projection of a 2D QMAT/QCPMG spectrum.

Finally, the dominance of the pyrosilicate $[Si_2O_7]^{6-}$ units in these Sc-silicate glasses is also evident in their Raman spectra (Figure 7). These spectra are dominated by a low-frequency band centered at 400 cm^{-1} with a weak shoulder in the mid-frequency range near 700 cm^{-1} and a high-frequency envelope that peaks near 900 cm^{-1} with a shoulder in the region between 950 and 1000 cm^{-1}. On the basis of previous Raman spectroscopic studies of crystalline rare-earth silicates of the stoichiometry $RE_2Si_2O_7$ including that of $Sc_2Si_2O_7$, these Raman bands can be assigned to the various vibrational modes of the $[Si_2O_7]^{6-}$ anionic units as follows [40–42]. The high-frequency bands near 900 and 950–1000 cm^{-1} correspond, respectively, to the symmetric and anti-symmetric stretching modes of the $Si(NBO)_3$ moieties of the two SiO_4 tetrahedra in the pyrosilicate unit. The weak mid-frequency shoulder near 700 cm^{-1} corresponds to the symmetric vibration of the Si–BO–Si linkage in this unit. Moreover, the spectral line shapes in Figure 7 are similar to that reported by Voron'ko et al. for a pyrosilicate melt of composition $Lu_2Si_2O_7$ [40]. It may be noted here that previous Raman spectroscopic studies on pyrosilicates indicated a negative correlation between the frequency of this band and the associated ∠Si–O–Si. According to this correlation, the location of the band near 700 cm^{-1} in the Raman spectra of these Sc-silicate glasses corresponds to an ∠Si–O–Si of ~130°, similar to that that observed in crystalline $La_2Si_2O_7$ and to be contrasted with an ∠Si–O–Si of 180° that is characteristic of crystalline $Sc_2Si_2O_7$. This result is consistent with the conclusions drawn from the ^{29}Si NMR results, as discussed above. Finally, the lowest frequency band near 400 cm^{-1} in the Raman spectrum in Figure 7 may correspond to the Si–O–Si bending mode as well as to Sc–O stretching of the ScO_6 octahedra in the structure.

Therefore, when taken together, the NMR and Raman spectroscopic results suggest that the structure of the Sc-37 and Sc-39

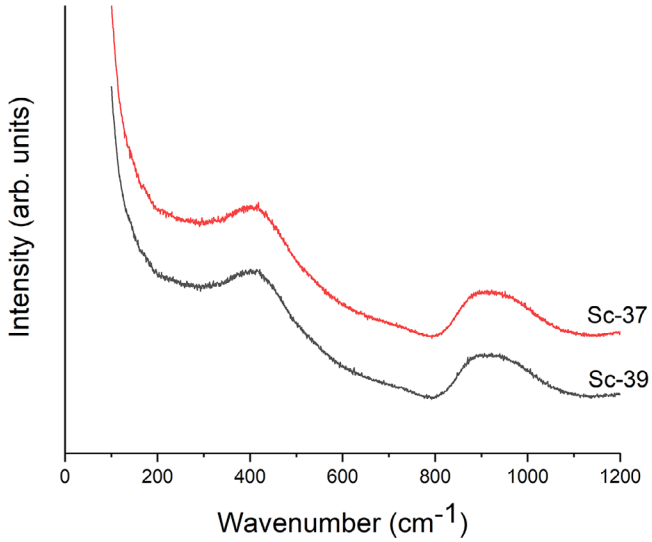

FIGURE 7 | Unpolarized Raman spectrum of Sc-37 (top) and Sc-39 (bottom) glasses.

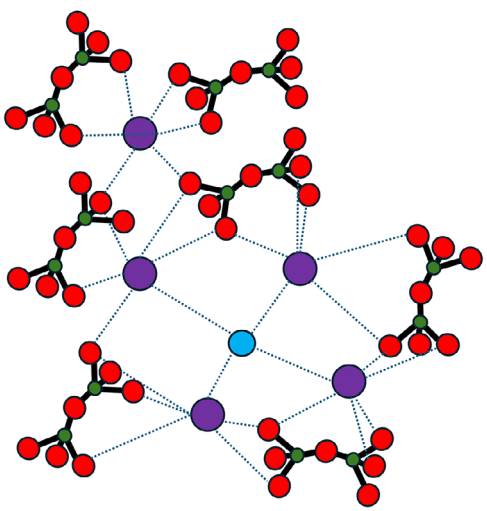

FIGURE 8 | Schematic ball-and-stick representation of structure of Sc-silicate glasses investigated in this study. Si, O, and Sc atoms are shown in green, red, and purple, respectively. FO atom in Sc–O–Sc environment is shown in teal.

glasses is dominated by $[Si_2O_7]^{6-}$ anionic units that are linked to one another via ScO_6 octahedra, whereas a small fraction of the structure also consists of Sc–O polyhedra connected via Sc–O–Sc linkages (Figure 8). Glass formation over such a narrow composition range in an RE_2O_3–SiO_2 system such as Sc_2O_3–SiO_2 is rather intriguing, especially when one considers the highly depolymerized structure of these glasses. The composition and structure of these glasses as well as the Sc_2O_3–SiO_2 phase diagram (Figure 1) suggest that upon supercooling their parent melts would rapidly crystallize the $Sc_2Si_2O_7$ pyrosilicate phase. We hypothesize that such crystallization is averted by the oxygen disproportionation reaction: 2NBO → FO + BO in the melt, which results in a structure that is structurally sufficiently frustrated to avert the rearrangement of oxygen atoms into a crystalline pyrosilicate structure with BO:NBO in 1:6 ratio with the complete absence of FO. Although this disproportionation reaction is expected to be entropically promoted at high temperature, it will also be favored by an increased field strength of the RE cation. Therefore, it will be interesting to explore in future studies the role of the latter parameter in controlling the glass-forming ability in other RE_2O_3–SiO_2 systems. Glass formation in the Sc_2O_3–SiO_2 system becomes more difficult with either increasing or decreasing Sc_2O_3 content outside the range of 37–39 mol%. It is likely that the lowering of the glass-forming ability with increasing Sc_2O_3 content is associated with the progressive depolymerization of the structure and creation of isolated SiO_4 tetrahedra. On the other hand, a decrease in the Sc_2O_3 content would promote liquid-liquid immiscibility that may drive nucleation and crystallization, thereby lowering the glass-forming ability.

4 | Summary

This study demonstrates that glass formation by containerless laser melt-quenching is possible in the binary Sc_2O_3–SiO_2 system, albeit within a very narrow compositional window (37–39 mol% Sc_2O_3) near a deep eutectic, despite the strong tendency of rare-earth silicates toward immiscibility and crystallization. Multinuclear NMR and Raman spectroscopic results reveal a highly depolymerized structure of these glasses, dominated by pyrosilicate $[Si_2O_7]^{6-}$ units that are connected via Si–O–Sc linkages with ScO_6 octahedra. Additionally, nearly 6% of the oxygen being present in $O(Sc)_4$ FO environment, a fraction of these ScO_6 octahedra are also connected with one another via Sc–O–Sc linkages. The high field strength of Sc^{3+} stabilizes the FO species via driving the oxygen disproportionation reaction: 2NBO → FO + BO. We propose that this oxygen disproportionation plays an important role in the (meta)stabilization of supercooled liquids near the deep eutectic against crystallization of the stable pyrosilicate phase, enabling glass formation despite the otherwise poor glass-forming ability of the system.

Acknowledgments

This work was supported by an NSF grant (DMR 2409281) to S.S. We thank Dr. Ping Yu at the NMR Facility at UC Davis for NMR data collection at low field and Dr. Taemin Yeo for collection of DSC scans. The National High Magnetic Field Laboratory is supported by the National Science Foundation through NSF/DMR-2128556 and the State of Florida.

Data Availability Statement

The data that support the findings of this study are available on request from the corresponding author. The data are not publicly available due to privacy or ethical restrictions.

References

1. J. E. Shelby, "Rare Earths as Major Components in Oxide Glasses," *KEM* 94–95 (1994): 1–42, https://doi.org/10.4028/www.scientific.net/KEM.94-95.1.

2. A. Makehima, Y. Tamura, and T. Sakaino, "Elastic Moduli and Refractive Indices of Aluminosilicate Glasses Containing Y_2O_3, La_2O_3, and TiO_2," *Journal of the American Ceramic Society* 61, no. 5–6 (1978): 247–249, https://doi.org/10.1111/j.1151-2916.1978.tb09291.x.

3. S. Iftekhar, J. Grins, P. N. Gunawidjaja, and M. Edén, "Glass Formation and Structure–Property–Composition Relations of the RE_2O_3–Al_2O_3–SiO_2 (RE = La, Y, Lu, Sc) Systems," *Journal of the American Ceramic Society* 94, no. 8 (2011): 2429–2435, https://doi.org/10.1111/j.1551-2916.2011.04548.x.

4. B. Pahari, S. Iftekhar, A. Jaworski, et al., "Composition-Property-Structure Correlations of Scandium Aluminosilicate Glasses Revealed by Multinuclear ^{45}Sc, ^{27}Al, and ^{29}Si Solid-State NMR," *Journal of the American Ceramic Society* 95, no. 8 (2012): 2545–2553, https://doi.org/10.1111/j.1551-2916.2012.05288.x.

5. Q. Shi, J. Kang, Y. Qu, et al., "Effect of Rare-Earth Oxides on Structure and Chemical Resistance of Calcium Aluminophosphate Glasses," *Journal of Non-Crystalline Solids* 491 (2018): 71–78, https://doi.org/10.1016/j.jnoncrysol.2018.04.010.

6. P. Yasaka and J. Kaewkhao, "Luminescence From Lanthanides-Doped Glasses and Applications: A Review," in 2015 *4th International Conference on Instrumentation, Communications, Information Technology, and Biomedical Engineering (ICICI-BME)* (IEEE, 2015), https://doi.org/10.1109/ICICI-BME.2015.7401304.

7. W. A. Pisarski, "Rare Earth Doped Glasses/Ceramics: Synthesis, Structure, Properties and Their Optical Applications," *Materials* 15, no. 22 (2022): 8099, https://doi.org/10.3390/ma15228099.

8. S. Sasaki, A. Masuno, K. Ohara, et al., "Structural Origin of Additional Infrared Transparency and Enhanced Glass-Forming Ability in Rare-Earth-Rich Borate Glasses Without B–O Networks," *Inorganic Chemistry* 59, no. 19 (2020): 13942–13951, https://doi.org/10.1021/acs.inorgchem.0c01567.

9. S. Sasaki, K. Tanaka, and A. Masuno, "Magneto-Optical Effect of Rare-Earth-Rich Borate Glasses Prepared Using a Levitation Technique," *Journal of the American Ceramic Society* 107, no. 12 (2024): 8126–8131, https://doi.org/10.1111/jace.20065.

10. A. Masuno, "Functionalities in Unconventional Oxide Glasses Prepared Using a Levitation Technique," *Journal of the Ceramic Society of Japan* 130, no. 8 (2022): 563–574, https://doi.org/10.2109/jcersj2.22073.

11. D. C. Kaseman, A. Retsinas, A. G. Kalampounias, G. N. Papatheodorou, and S. Sen, "Q-Speciation and Network Structure Evolution in Invert Calcium Silicate Glasses," *Journal of Physical Chemistry B* 119, no. 26 (2015): 8440–8445, https://doi.org/10.1021/acs.jpcb.5b02469.

12. J. Wu and J. F. Stebbins, "Effects of Cation Field Strength on the Structure of Aluminoborosilicate Glasses: High-Resolution 11B, 27Al and 23Na MAS NMR," *Journal of Non-Crystalline Solids* 355, no. 9 (2009): 556–562, https://doi.org/10.1016/j.jnoncrysol.2009.01.025.

13. R. K. Swanson, J. F. Stebbins, T. M. Yeo, et al., "Structure and Fragility of Normal and Invert Lanthanum Borate Glasses: Results From 11B and 17O NMR Spectroscopy and Calorimetry," *Journal of Non-Crystalline Solids* 603 (2023): 122119, https://doi.org/10.1016/j.jnoncrysol.2022.122119.

14. S. K. Lee and E. J. Kim, "Probing Metal-Bridging Oxygen and Configurational Disorder in Amorphous Lead Silicates: Insights From ^{17}O Solid-State Nuclear Magnetic Resonance," *Journal of Physical Chemistry C* 119, no. 1 (2015): 748–756, https://doi.org/10.1021/jp509780f.

15. I. Hung, Z. Gan, P. L. Gor'kov, et al., "Detection of "Free" Oxide Ions in Low-Silica Ca/Mg Silicate Glasses: Results From ^{17}O→^{29}Si HETCOR NMR," *Journal of Non-Crystalline Solids* 445–446 (2016): 1–6, https://doi.org/10.1016/j.jnoncrysol.2016.04.042.

16. X. Chen, F. Wang, W. Zhi, et al., "Phase Equilibria of the CaO–SiO_2–Sc_2O_3 Ternary System," *Journal of Phase Equilibrium and Diffusion* 44, no. 1 (2023): 102–114, https://doi.org/10.1007/s11669-022-01022-y.

17. K. Qi, C. Liao, Z. Pi, and F. Zhang, "Thermodynamic Modeling of Phase Diagrams in La_2O_3–SiO_2, Dy_2O_3–SiO_2 and Er_2O_3–SiO_2 Systems," *Calphad* 87 (2024): 102750, https://doi.org/10.1016/j.calphad.2024.102750.

18. L. A. Makrovets, "Y_2O_3–SiO_2 Phase Diagram," *Russian Metallurgy* 2023, no. 8 (2023): 1155–1158, https://doi.org/10.1134/S0036029523080141.

19. V. K. Cherepanova and A. N. Cherepanov, "A Mathematical Model of Scandium Ore Deposit Formation in Liquating Magmatic Melts," *Thermophysics and Aeromechanics* 24, no. 2 (2017): 309–322, https://doi.org/10.1134/S0869864317020147.

20. F. Auzel and P. Goldner, "Towards Rare-Earth Clustering Control in Doped Glasses," *Optical Materials* 16, no. 1–2 (2001): 93–103, https://doi.org/10.1016/S0925-3467(00)00064-1.

21. A. Vonderhaar, M. P. Stone, J. Campbell, T. W. Hawkins, J. Ballato, and P. D. Dragic, "Concentration Quenching and Clustering Effects in Er:YAG-Derived All-Glass Optical Fiber," *Optical Materials Express* 11, no. 10 (2021): 3587, https://doi.org/10.1364/OME.437825.

22. J. F. Stebbins, P. Zhao, S. Keun Lee, and J. V. Oglesby, "Direct Observation of Multiple Oxygen Sites in Oxide Glasses: Recent Advances From Triple-Quantum Magic-Angle Spinning Nuclear Magnetic Resonance," *Journal of Non-Crystalline Solids* 293–295 (2001): 67–73, https://doi.org/10.1016/S0022-3093(01)00653-6.

23. J. A. Tangeman, B. L. Phillips, A. Navrotsky, J. K. R. Weber, A. D. Hixson, and T. S. Key, "Vitreous Forsterite (Mg_2SiO_4): Synthesis, Structure, and Thermochemistry," *Geophysical Research Letters* 28, no. 13 (2001): 2517–2520, https://doi.org/10.1029/2000GL012222.

24. M. D. Alba, P. Chain, P. Florian, and D. Massiot, "^{45} Sc Spectroscopy of Solids: Interpretation of Quadrupole Interaction Parameters and Chemical Shifts," *Journal of Physical Chemistry C* 114, no. 28 (2010): 12125–12132, https://doi.org/10.1021/jp1036525.

25. I. Hung, T. Edwards, S. Sen, and Z. Gan, "MATPASS/CPMG: A Sensitivity Enhanced Magic-Angle Spinning Sideband Separation Experiment for Disordered Solids," *Journal of Magnetic Resonance* 221 (2012): 103–109, https://doi.org/10.1016/j.jmr.2012.05.013.

26. N. M. Trease, K. K. Dey, and P. J. Grandinetti, "Optimum Excitation of "Enhanced" Central Transition Populations," *Journal of Magnetic Resonance* 200, no. 2 (2009): 334–339, https://doi.org/10.1016/j.jmr.2009.07.020.

27. S. P. Brown and S. Wimperis, "Two-Dimensional Multiple-Quantum MAS NMR of Quadrupolar Nuclei. Acquisition of the Whole Echo," *Journal of Magnetic Resonance* 124, no. 1 (1997): 279–285, https://doi.org/10.1006/jmre.1996.1059.

28. Z. Gan and H.-T. Kwak, "Enhancing MQMAS Sensitivity Using Signals From Multiple Coherence Transfer Pathways," *Journal of Magnetic Resonance* 168, no. 2 (2004): 346–351, https://doi.org/10.1016/j.jmr.2004.03.021.

29. I. Hung and Z. Gan, "A Magic-Angle Turning NMR Experiment for Separating Spinning Sidebands of Half-Integer Quadrupolar Nuclei," *Chemical Physics Letters* 496, no. 1–3 (2010): 162–166, https://doi.org/10.1016/j.cplett.2010.07.016.

30. R. K. Harris, E. D. Becker, S. M. Cabral De Menezes, R. Goodfellow, and P. Granger, "NMR Nomenclature. Nuclear Spin Properties and Conventions for Chemical Shifts (IUPAC Recommendations 2001)," *Pure and Applied Chemistry* 73, no. 11 (2001): 1795–1818, https://doi.org/10.1351/pac200173111795.

31. A. Jaworski, B. Stevensson, and M. Edén, "The Bearings From Rare-Earth (RE = La, Lu, Sc, Y) Cations on the Oxygen Environments in Aluminosilicate Glasses: A Study by Solid-State ^{17}O NMR, Molecular Dynamics Simulations, and DFT Calculations," *Journal of Physical Chemistry C* 120 (2016), 13181–13198, https://doi.org/10.1021/acs.jpcc.6b02032.

32. J.-P. Amoureux, C. Huguenard, F. Engelke, and F. Taulelle, "Unified Representation of MQMAS and STMAS NMR of Half-Integer Quadrupolar Nuclei," *Chemical Physics Letters* 356, no. 5–6 (2002): 497–504, https://doi.org/10.1016/S0009-2614(02)00398-6.

33. P. Guerry, D. L. Carroll, P. N. Gunawidjaja, et al., "Solid State NMR as a Probe of Inorganic Materials: Examples From Glasses and Sol-Gels," *MRS Online Proceedings Library* 984 (2006): 1201, https://doi.org/10.1557/PROC-984-0984-MM12-01.

34. Y. Kholina, J. Ren, C. Doerenkamp, et al., "Local Structural Environments in Cubic Sr_2ScGaO_5 : A Multinuclear Solid-State NMR Study,"

Journal of Physical Chemistry C 129, no. 49 (2025): 21728–21737, https://doi.org/10.1021/acs.jpcc.5c03744.

35. M. Magi, E. Lippmaa, A. Samoson, G. Engelhardt, and A. R. Grimmer, "Solid-State High-Resolution Silicon-29 Chemical Shifts in Silicates," *Journal of Physical Chemistry* 88, no. 8 (1984): 1518–1522, https://doi.org/10.1021/j150652a015.

36. A. Jaworski, T. Charpentier, B. Stevensson, and M. Edén, "Scandium and Yttrium Environments in Aluminosilicate Glasses Unveiled by $^{45}Sc/^{89}Y$ NMR Spectroscopy and DFT Calculations: What Structural Factors Dictate the Chemical Shifts?," *Journal of Physical Chemistry C* 121, no. 34 (2017): 18815–18829, https://doi.org/10.1021/acs.jpcc.7b05471.

37. M. Wierzbicka-Wieczorek, U. Kolitsch, and E. Tillmanns, "The Crystal Structures of Three New Complex Silicates of Scandium," *Canadian Mineralogist* 48, no. 1 (2010): 51–68, https://doi.org/10.3749/canmin.48.1.51.

38. I. D. Brown, "Recent Developments in the Methods and Applications of the Bond Valence Model," *Chemical Reviews* 109, no. 12 (2009): 6858–6919, https://doi.org/10.1021/cr900053k.

39. I. D. Brown, "The Bond-Valence Method: An Empirical Approach to Chemical Structure and Bonding," *Industrial Chemistry Library* 2 (1981): 1–30, https://doi.org/10.1016/B978-0-12-525102-0.50007-4.

40. Y. K. Voron'ko, A. A. Sobol', V. E. Shukshin, and Y. V. Gerasimov, "Spontaneous Raman Scattering of $Lu_2Si_2O_7$ Single Crystals at Temperatures in the Range From 20 to 2173 K," *Physics of the Solid State* 57, no. 7 (2015): 1424–1430, https://doi.org/10.1134/S1063783415070367.

41. F. Bretheau-Raynal, J. P. Dalbiez, M. Drifford, and B. Blanzat, "Raman Spectroscopic Study of Thortveitite Structure Silicates," *Journal of Raman Spectroscopy* 8, no. 1 (1979): 39–42, https://doi.org/10.1002/jrs.1250080110.

42. J. H. Denning, R. F. Hudson, D. R. Laughlin, S. D. Ross, and A. M. Sparasci, "The Vibrational Spectra of Some Rare-Earth Pyrosilicates," *Spectrochimica Acta Part A: Molecular Spectroscopy* 28, no. 9 (1972): 1787–1791, https://doi.org/10.1016/0584-8539(72)80149-1.